Supplement of

Brief Communication: Heterogenous thinning and disconnected subglacial lake filling observed on Thwaites Glacier, West Antarctica

Andrew O. Hoffman et al.

5   *Correspondence to*: Andrew O. Hoffman (hoffmaao@uw.edu)

1 Introduction

Here we provide additional information on glaciostatic hydropotential time series, water routing, and describe the diagnostic model simulations we use to interrogate the influence of lake fill-drain cycles on basal resistance and ice sliding velocity.

2 Lake volume change

10   We applied the same SAR LOS methods to measure vertical displacements on the lakes identified by Smith et al. (2017) to estimate lake volume change on the lakes identified in the western Haynes Glacier shear margin (Fig. S1). We also create average lake volume change estimates from the gridded CryoSat-2 time series (Fig. S2).
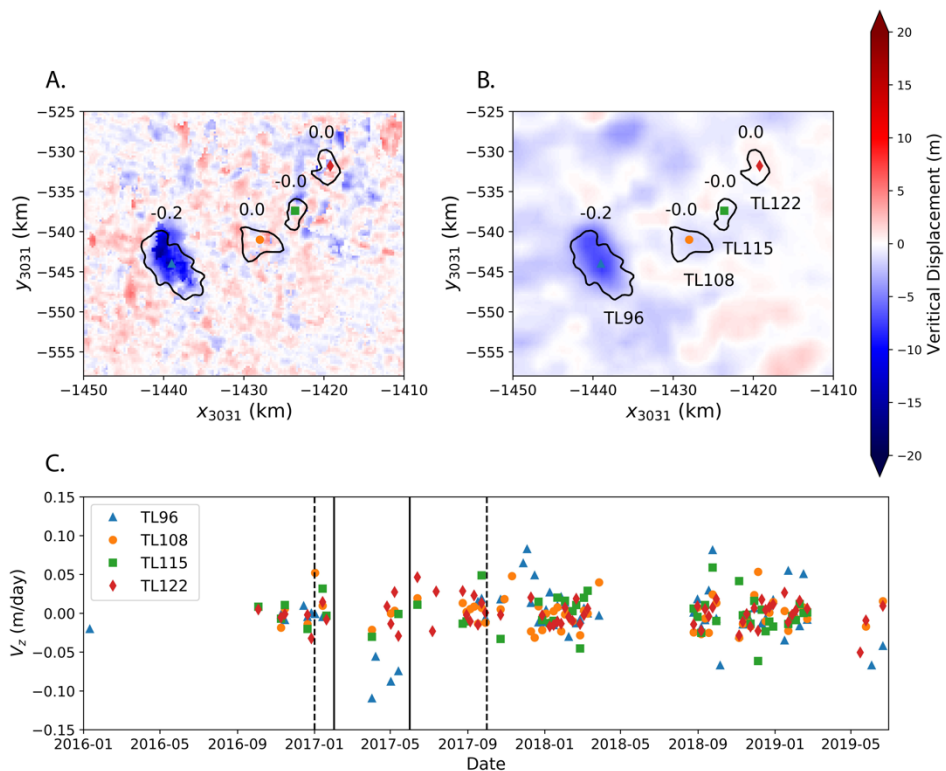
Supplement figure 1: SAR-derived surface elevation change time series over the Haynes Glacier lakes. Solid lines represent the mean time of SAR elevation mosaic differenced to create panel A and B. Dotted lines represent the quarters of gridded CryoSat-2 data differenced to create figure 1b. Numbers next to each lake represent volume flux change (km³) over integrated period.
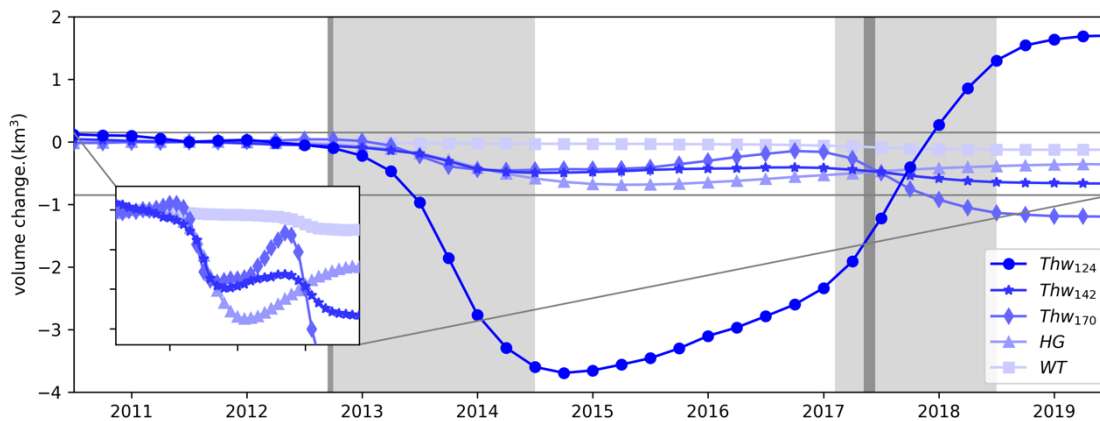
Supplement figure 2: Volume change over complete observation period derived from CryoSat-2 data by subtracting an average thinning rate outside the lake from average elevation change in the lake and multiplying by the lake area.

3 Hydropotential, water routing, and lake volume change

From the CryoSat-2 elevation change time series, we construct quarterly models of glaciostatic hydraulic potential. We first
25   calculate a reference elevation model associated with the drained lakes. In the footprint of the lakes, anomalous height change
relative to background thinning is linked to filling and draining of subglacial water. We estimate the glaciostatic hydropotential
as

$$\phi_q = P_q + \rho_{water}gz$$

where the water pressure at each quarter, P_q, is assumed to be near the sum of the overburden stress of ice and lake water
30   thickness, H_q and h_q, respectively:

$$P_q \cong \rho_{ice}gH_q + \rho_{ice}gh_q$$

We then derive subglacial water fluxes multiplying the flow accumulation associated with the hydraulic potential time series
by the distributed melt field derived by Joughin et al (2009). We assume the melt rates are stationary relative to the ongoing
35   thinning and derive water routing beneath Thwaites Glacier (see supplement movie). The water routing between the lakes
remains relatively constant, despite a general increase the hydraulic potential difference between the lakes as the lower reaches
of Thwaites Glacier thin and changes as lakes fill and drain.
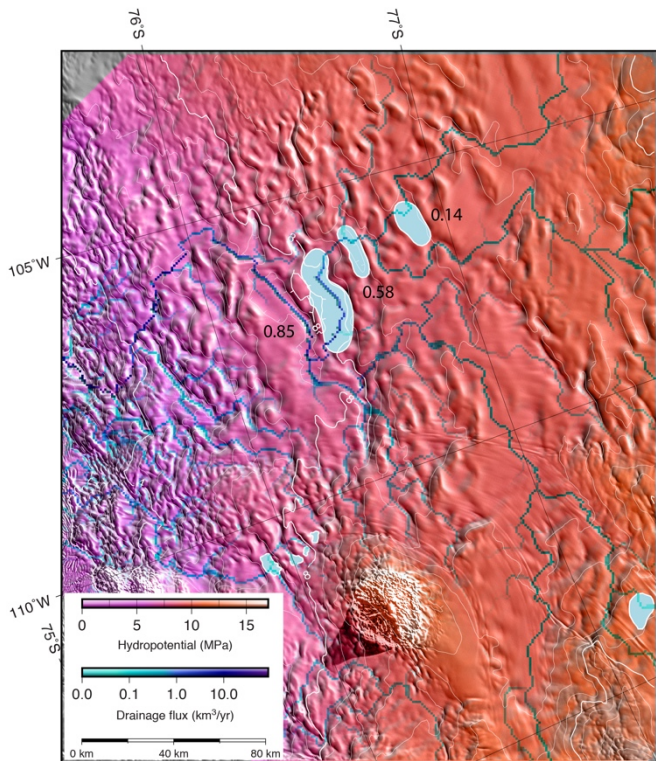
Supplement figure 3: Average water flux assuming static hydropotential and basal melt rates from Joughin et al. (2009). Supplement movie shows weak sensitivity for water rerouting as the glacier thins and lakes fill and drain. The cumulative water fluxes (km³/yr) into lakes Thw124,142,170 are printed with each lake.

4 Inversions of basal friction

Modelled ice temperature depends on the inferred basal shear stress and ice viscosity because of their combined effect on frictional and strain heating near the bed. Ice viscosity is best described by a temperature-dependent Arrhenius relation, making simultaneous inferences of ice rheology and basal friction difficult to separate from snap-shot observations of ice thickness and velocity. In our diagnostic inversions for bed friction and the enhancement factor, we use the ice-flow model icepack (doi:10.5281/zenodo.3542092) to solve the weak form of the shallow-shelf equations (Bueler et al., 2009), modified to include frictional energy dissipation:

$$F(u) = \int_\Omega \tau \left(\left(u_0^{\frac{1}{m}+1} + |u|^{\frac{1}{m}+1} \right)^{\frac{m}{m}+1} - u_0 \right) dx.$$

This functional describes the stress accommodation of the bed assuming a regularized Coulomb friction law (Joughin et al., 2019). We iteratively refine our proxies for bed resistance, $\tau = \tau_0 e^\beta$, and the fluidity in Glen's flow law, $A = A_0 e^\theta$, using the Gauss-Newton method to perturb parameters β and θ to minimize the objective functional:

$$E(u) = \int_{\Omega} \left(\frac{u - u_{obs}}{\sigma} \right)^2 dx,$$

where u are the modelled velocities and σ are the standard deviations of the measured inSAR velocities, u_{obs}. In our iterative
55   inversion scheme, we first calculate the depth-averaged enhancement factor from the 3D temperatures derived by Van
Liefferinge and Pattyn (2013) and use this initial estimate to infer an initial basal shear stress field. For the floating eastern
Thwaites Ice Shelf where we do not have independently modelled ice temperatures, we assume a constant viscosity before
advecting the initial temperature solution through the shelf (~20 years of spin up). We do not include the rifted western
Thwaites Ice Shelf in our model domain because we find it provides almost no backstress to grounded ice (Luchitta et al.,
60   1993, Reese et al., 2017). Because almost all relative motion is accommodated by sliding in the shallow-shelf equations, our
procedure overestimates shear stress at the ice-bed interface; however, our interest in differences between two representative
model periods (before and after the lakes drain) makes this model assumption less impactful. Figure S4 shows the results of
these simulations where deviations of shear stress inside the lake are smaller than outside the lake.

65
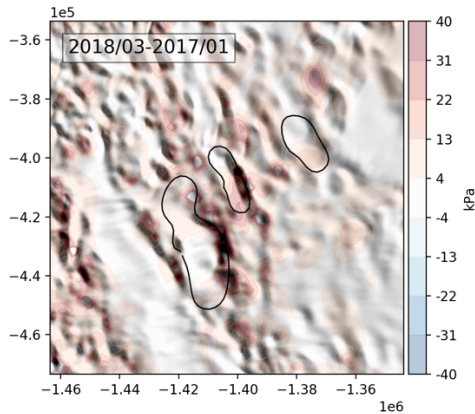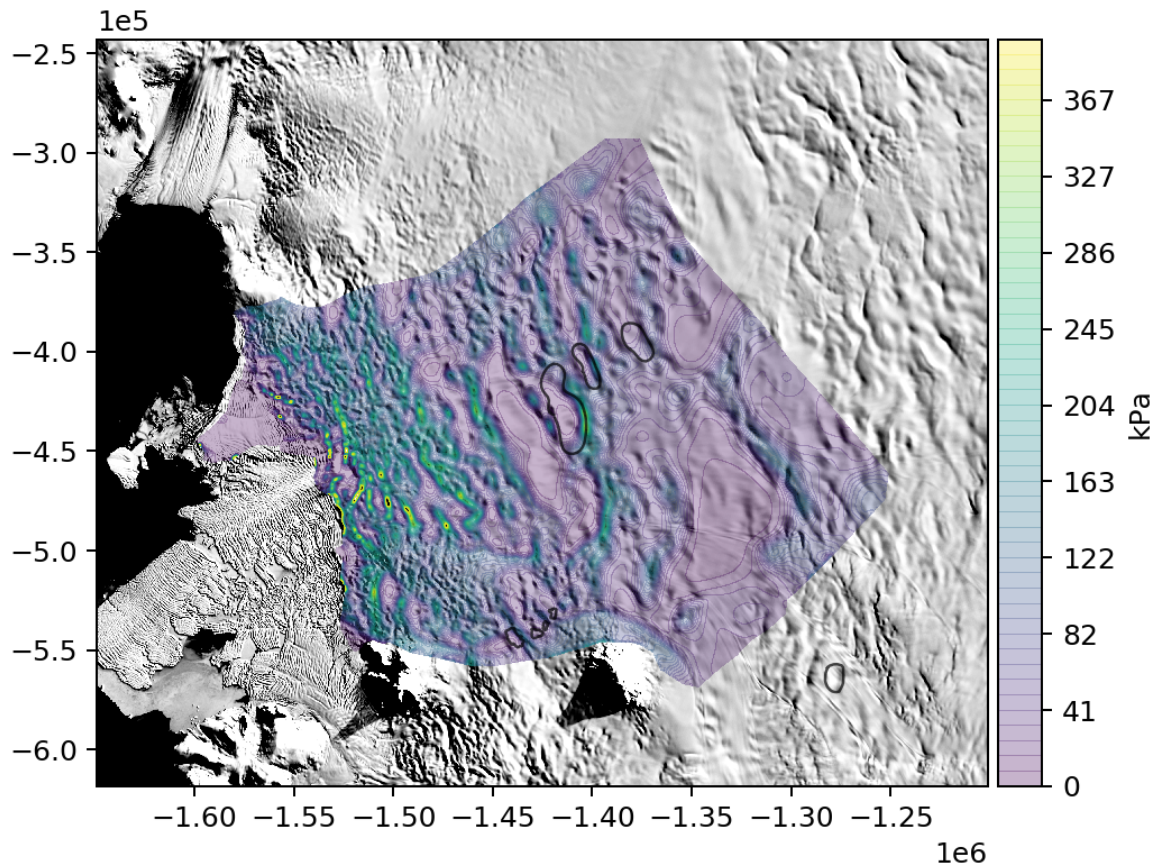
Supplement figure 4: Static inversion for basal resistance field for 2017 catchment geometry before the Haynes Glacier and Thwaites Glacier drainage events. Panelled image shows difference in inferred basal resistance between two static inversions from 2017 and 2018 for Thw$_{124,142,170}$.

References

Bueler E., Brown, J.: Shallow shelf approximation as a sliding law in a thermodynamically coupled ice sheet model, . J. Geophys. Res, 114, F1, 2009. doi:10.1029/2008JF001179

Joughin, I., Tulaczyk, S., Bamber, J., Blankenship, D., Holt, J., Scambos, T., & Vaughan, D.: Basal conditions for Pine Island and Thwaites Glaciers, West Antarctica, determined using satellite and airborne data. Journal of Glaciology, *55*(190), 245-257, 2009. doi:10.3189/002214309788608705

Joughin, I., Smith, B., and Schoof, C.: 2019. Regularized Coulomb Friction Laws for Ice Sheet Sliding: Application to Pine
80   Island Glacier, Antarctica. Geophy Res. Lett., 46, 4764–4771. doi:10.1029/2019GL082526

Lucchitta, B., Mullins, K, Allison, A., & Ferrigno, J. (1993). Antarctic glacier-tongue velocities from Landsat images: First
results. Annals of Glaciology, 17, 356-366. doi:10.3189/S0260305500013100

85   Reese R., Gudmundsson G.H., Levermann, A., Winkelmann, R.: The far reach of ice-shelf thinning in Antarctica, Nature
Climate Change, 8, 53-57, 2018. doi:10.1038/s41558-017-0020-x

Van Liefferinge B., and Pattyn F., Using ice-flow models to evaluate potential sites of million-year-old ice in Antarctica, Clim.
Past, 9, 2335-2345, 2013. doi:10.5194/cp-2335-2013
90